 doi:10.20944/preprints202106.0143.v1

Article

Changes in Power Plant NO_x Emissions over Northwest Greece Using a Data Assimilation Technique

Ioanna Skoulidou[1]*, Maria-Elissavet Koukouli[1], Arjo Segers[2], Astrid Manders[2], Dimitris Balis[1], Trisevgeni Stavrakou[3], Jos van Geffen[4] and Henk Eskes[4]

[1] Laboratory of Atmospheric Physics, Aristotle University of Thessaloniki, Thessaloniki, Greece
[2] TNO, Climate, Air and Sustainability, Utrecht, the Netherland
[3] Royal Belgian Institute for Space Aeronomy (BIRA-IASB), Brussels, Belgium
[4] Royal Netherlands Meteorological Institute (KNMI), De Bilt, the Netherlands

* Correspondence: ioannans@auth.gr

Abstract: In this work, we investigate the ability of a data assimilation technique and space-borne observations to quantify and monitor changes in nitrogen oxides (NO_x) emissions over North-Western Greece for the summers of 2018 and 2019. In this region, four lignite-burning power plants are located. The data assimilation technique, based on the Ensemble Kalman Filter method, is employed to combine space-borne atmospheric observations from the high spatial resolution Sentinel-5 Precursor (S5P) Tropospheric Monitoring Instrument (TROPOMI) and simulations using the LOTOS-EUROS Chemical Transport model. The Copernicus Atmosphere Monitoring Service-Regional European emissions (CAMS-REG, version 4.2) inventory based on year 2015 is used as the *a priori* in the simulations. Surface measurements of nitrogen dioxide (NO_2) from air quality stations operating in the region are compared with the model surface NO_2 output using either the *a priori* (base run) or the *a posteriori* (assimilated run) NO_x emissions. The high biases found between the in situ NO_2 measurements and the base run surface NO_2 decrease in the assimilated run in most cases. The bias in the station near the largest power plant decreases to 2.0 μg/m^3 (2.83 μg/m^3) from 10.5 μg/m^3 (8.46 μg/m^3) in 2019 (2018 respectively). Concerning the estimated annual *a posteriori* NO_x emissions it was found that, for the pixels hosting the two largest power plants, the assimilated run results in emissions decreased by ~40-50% for 2018 compared to 2015, whereas a larger decrease, of ~70% for both power plants, was found for 2019, after assimilating the space-born observations. For the same power plants, the European Pollutant Release and Transfer Register (E-PRTR) reports decreased emissions in 2018 and 2019 compared to 2015 (-35% and -38% in 2018, -62% and -72% in 2019), in good agreement with the estimated emissions. We further compare the *a posteriori* emissions to the reported energy production of the power plants during the summer of 2018 and 2019. Mean decreases of about -35% and-63% in NO_x emissions are estimated for the two larger power plants in summer of 2018 and 2019, respectively, which are supported by similar decreases in the reported energy production of the power plants (~-30% and -70%, respectively).

Keywords: Data assimilation; TROPOMI; Air Quality modelling; NOx Emissions; Ensemble Kalman Filter; LOTOS-EUROS; power plant; anthropogenic

1. Introduction

Emissions of nitrogen oxides ($NO_x = NO + NO_2$) play a pivotal role in local and global atmospheric composition and air quality. NO_x contributes to the formation of tropospheric ozone, peroxyacyl nitrate (PAN) and nitrate aerosols, and contributes to the environmental acidification [1]. Fossil fuel combustion, mainly originating from power plants, transport and industry, are the main anthropogenic sources of NO_x in the atmosphere, while NO_x is naturally emitted from soil, biomass burning and lightning [2]. Primarily,

NO_x is released in the form of NO that rapidly reacts with ozone and transforms into NO_2, which is photodissociated during daytime.

The current anthropogenic emission inventories generally rely on the "bottom-up" approach, which uses geographical and statistical data [3,4]. Due to low temporal and spatial resolution of the underlying data, these estimates are highly uncertain. In addition, the input data for an inventory is usually not available in near-real-time but is only completed with a delay of at least one or more years. Unfortunately, rapid changes in tropospheric NO_2 levels have been observed and have been attributed to both environmental policy measures [5,6] and global crises, such as the current COVID-19 pandemic [7,8]. A bottom-up emission inventory is understandably unable to represent such changes if it is used in studies that refer to recent years with such strong changes.

In a "top-down" approach, the discrepancy between chemical model predictions and space-borne atmospheric observations is minimized to find the best matching emissions. This approach is gaining more and more ground since satellite observations of improved quality and spatial coverage become available. In recent years, the methods employed to reduce the discrepancies between model and observations are advanced data assimilation techniques and use either in situ observations [9] or satellite retrievals [2,4]. The Ensemble Kalman Filter (EnKF) is such a data assimilation technique [10] that has already been employed in different atmospheric studies.

In the current study, we estimate NO_x emission changes in Northwest Greece based on the high spatial resolution Sentinel-5 Precursor (S5P) Tropospheric Monitoring Instrument (TROPOMI) observations and simulations using the LOTOS-EUROS Chemical Transport model. The topography of Northwest Greece is shown in **Figure 1**. In the centre of the area, a basin is located in 650 m above mean sea level, which is about ~ 50 km long and 10 to 25 km wide, surrounded by mountains of around 1350 m above mean sea level. Inside the basin, small hills are present. Vegetation is restricted to isolated trees and small bushes [11]. Four lignite-burning power plants (annotated in **Figure 1**), operated by the Greek Public Energy Corporation, are located in this basin, and use lignite from nearby open-pit coal-mines. In terms of total installed capacity, the biggest plant is Ag. Dimitrios (~1450 MW; 40.3920°N, 21.9280°E), located in the southeast of the region, followed by Kardia (~1100 MW, 40.4089°N, 21.7857°E), Amyntaio (~550 MW, 40.6178°N, 21.6858°E) and Meliti (~290 MW, 40.8153°N, 21.59829°E). In addition, one more lignite power plant, near the city of Bitola (~680 MW), is operating close to the border with the neighboring Republic of North Macedonia. The climate of the area is continental Mediterranean, characterized by high temperatures in summer and low temperatures in winter, while the prevailing winds during summer in the centre of the basin are mainly of NW, NNW and WNW directions (16.4, 15.6, and 9.9%, respectively) [11]. Nevertheless, the wind direction in the southern part of the basin is NE, dominated by the topography of the region. The villages and towns located in and around the basin, and their population are also shown in **Figure 1**. Finally, the locations of in situ air quality stations operating in the area are represented by black dots on the map.

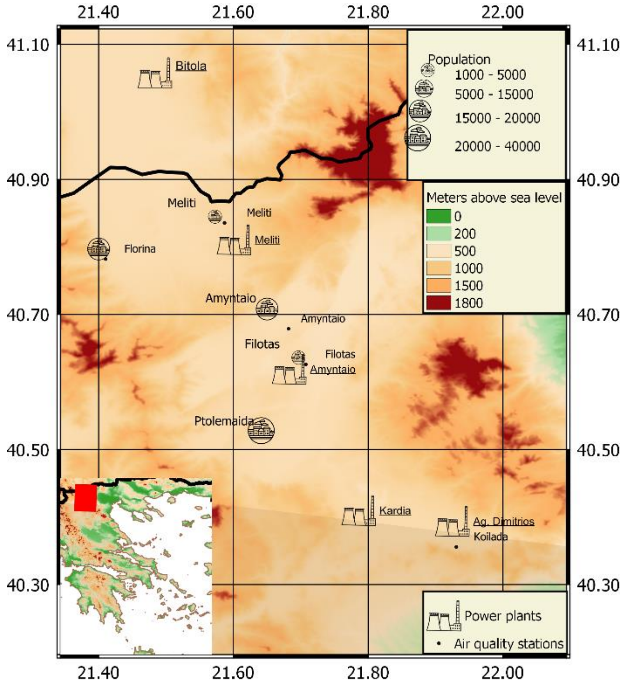

Figure 1. The topography of the target region with the location of the power plants, cities and towns, and air quality stations.

The Greek National Energy and Climate Plan (NCEP, https://ec.europa.eu/energy/sites/ener/files/el_final_necp_main_en.pdf) is a well-developed strategy that provides environmental objectives, policies and measures. The NCEP integrates the targets set in the Directive 2016/2284/EC concerning the reduction of national emissions of certain atmospheric pollutants, such as NO_x, SO_2 and NMVOC. Greece's commitment regarding NO_x emissions is a reduction of 31% for the period between 2020 and 2029 and a reduction of 55% after 2030 compared to 2005. According to the European Pollutant Release and Transfer Register (E-PRTR), the region of western Macedonia in Northwest Greece, reported the largest NO_x emissions from lignite power plants (about 60 kt) for 2007 followed by the Aegean Sea islands and Crete. NO_x emissions in the region of Northwest Greece are reported to decrease significantly in the following years, declining to ~17 kt in 2017.

The annual NO_x 2015-2019 emissions, reported in E-PRTR based on measurements of the NOx mass concentrations, for the four large power plants in the region of Northwest Greece (dotted lines in **Figure 2**) are largest for the Ag. Dimitrios power plant, followed by Kardia, Amyntaio and Meliti, in accordance with their installed capacity. The energy production of the power plants (solid lines in **Figure 2**), reported by the Energy Exchange Group-EnEx (www.enexgroup.gr), follows the variability of the emissions throughout the years, showing large decreases in energy production in 2019 mainly in the Ag. Dimitrios and Kardia plants. The important reduction of NO_x emissions in the region is further confirmed by NO_2 column measurements from the Ozone Monitoring Instrument (OMI) aboard of the EOS-Aura satellite [12]. The deseasonalized monthly tropospheric NO_2 columns at the satellite pixel where the large power plant of Ag. Dimitrios is located is shown in **Figure S1** (top) between 2005 and 2020. Especially after 2016, strong reduction in NO_2 levels is seen and corresponds very well with the reported decreases in **Figure 2**. The mean annual tropospheric NO_2 columns are shown in **Figure S1** (bottom) together with the corresponding trend showing a decrease of about 2.5×10^{15} molecules cm^{-2} (about -55%) per decade.

Preprints (www.preprints.org) | NOT PEER-REVIEWED | Posted: 4 June 2021 doi:10.20944/preprints202106.0143.v1

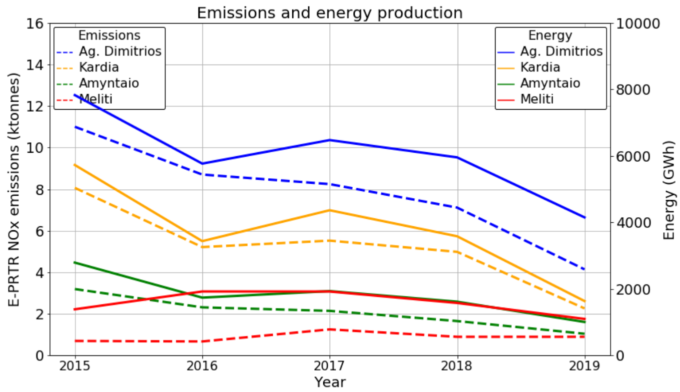

Figure 2. Annual NO_x emissions for the four power plants in the target region as reported by E-PRTR between 2015 and 2019 (dashed lines) and the annual energy from the power plants in the region over the same period (solid line) as reported by the Energy Exchange Group for the four power plants; Ag. Dimitrios (blue), Kardia (orange), Amyntaio (green) and Meliti (red).

In this work, the emissions are studied for the summer periods (i.e. June, July and August) of 2018 and 2019 and the data assimilation technique applied is a Local Ensemble Transform Kalman Filter system developed around the LOTOS-EUROS CTM. The study is conducted for the summer periods only, when satellite NOx time series are less susceptible to gaps due to cloudy days. Since the emissions reported by independent sources show an important decrease, even between the years 2018 and 2019, we study here the ability of the assimilation of satellite observations to sense these changes as well. Furthermore, the lignite plants in the region are major and relatively isolated sources of emissions, which renders them an appropriate candidate to apply such an assimilation technique.

After describing the different data sets and models used in this analysis, we present the comparisons between the CTM NO_2 columns for the summers of 2018 and 2019 and the TROPOMI tropospheric NO_2 observations. The simulations are based on an inventory for the year 2015, the most recent available at the time of study. We then show the improvement in these comparisons, after the TROPOMI observations are assimilated into the CTM. The changes in estimated emissions between years 2018, 2019 and 2015 compare with the changes reported in the E-PRTR emissions database for the four power plants for the same years. We further validate the LOTOS-EUROS surface NO_2 concentrations against in situ observations from air quality stations that are located near the power plants. Finally, the reported changes in the power plants' energy production is compared with the calculated changes in emissions found from the inversion algorithm, providing further validation of the emission levels from the power plants.

2. Materials and Methods

2.1. The LOTOS-EUROS CTM

The LOTOS-EUROS (Long Term Ozone Simulation – EURopean Operational Smog model) (https://lotos-euros.tno.nl/) simulates the air pollution in the troposphere while a detailed description of the model is available in [13]. LOTOS-EUROS is one of the nine state-of-the-art systems used in the operational Copernicus Atmosphere Monitoring Services (CAMS, https://atmosphere.copernicus.eu/). An extensive evaluation of the overall model performance over Greece using ground-based measurements and satellite derived observations has been performed by [14]. In summary, it has been found that the modelled NO_2 columns show a high spatial correlation (0.95) and a negative bias of -18% when compared with S5P/TROPOMI tropospheric columns over Athens in summertime. The *a priori* emission inventory and boundary layer height assumptions were found to be significant sources of uncertainty in model simulations.

In this study we use the model version 2.2.001. The simulations cover the domain in Northwest Greece (**Figure 3**) and expand from 40.2° to 41.2°N and 21.2° to 22.2°E. The horizontal spatial resolution is set to 0.1° longitude ×0.05° latitude (about 10 km x5 km at Greece latitudes). In the vertical, ten hybrid sigma-pressure layers are used with a top at about 200 hPa; these are obtained as a coarsening of the layers in the meteorological input. The gas phase chemistry follows a modified version of Carbon Bond Mechanism IV scheme (CBM-IV) [15] while the aerosol chemistry uses the ISORROPIA II parameterization [16]. Meteorological variables are obtained at 7km×7km spatial resolution from the Integrated Forecasting System (IFS) of the European Centre for Medium-Range Weather Forecasts (ECMWF). The surface-layer meteorological variables are obtained at hourly resolution while the 3-dimensional variables at model levels every 3 hours [17]. Boundary and initial conditions are obtained from the Copernicus Atmosphere Monitoring Service (CAMS, https://atmosphere.copernicus.eu/), global near-real time (NRT) product, at a 3-hour temporal resolution and a spatial resolution of about 35 km. Anthropogenic emissions are taken from the CAMS-REG (CAMS-Regional European emissions) inventory version 4.2 for the year 2015 [18] at a spatial resolution of 0.1° longitude and 0.05° latitude while the emissions temporal profiles used are the default provided with the inventory. The latest available year in this inventory is 2015, and this year is therefore used for the simulations in this study. Biogenic emissions are calculated online using actual meteorology and depend on a detailed land use and tree-species database described in [19]. Soil NO emissions are taken from a parametrization depending on soil type and soil temperature [20]. Emissions for lightning are not included in the simulations. Emissions from biomass burning are obtained from the Global Fire Assimilation System (GFAS) dataset [21].

2.2. *The a priori NOx emissions*

The total *a priori* anthropogenic and biogenic emissions, used for the simulations in summer 2019 are shown in **Figure 3.** The power plant locations are identified by the green star symbols. The black triangles represent cities, the size of the triangle is proportional to the population.

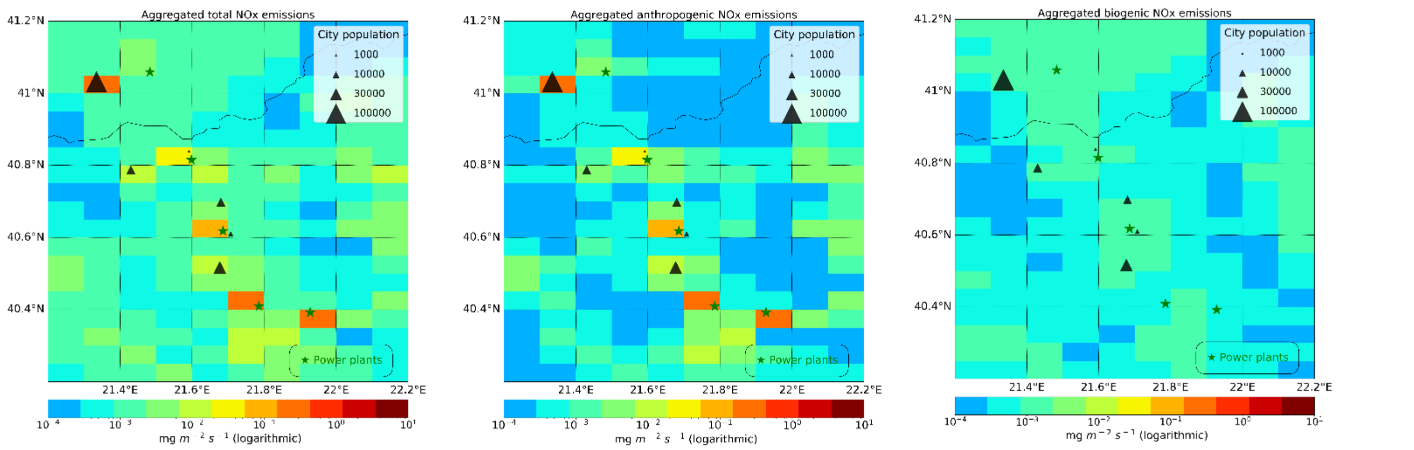

Figure 3. NO_x emissions used in the model in summer 2019. **(a)** Total emissions; **(b)** Anthropogenic emissions; **(c)** Biogenic emissions 2019.

The sum of the anthropogenic emissions in the grid-cells where the power plants are located constitute more than 95% of the total emissions (including biogenic), making anthropogenic the primary NO_x source in this region (**Figure 3**). The annual anthropogenic emissions from the point sources of public power sector in CAMS-REG over the pixels

 doi:10.20944/preprints202106.0143.v1

where the three larger power plants are located are by far dominant (> 96%) compared to the rest emitting anthropogenic sources (**Table 1**). In the grid pixel where the smaller capacity, Meliti, power plant is located, the rest of the emitting anthropogenic emissions account for about 15% of the total anthropogenic emissions.

Table 1. Annual NO_x emissions from CAMS-REG emission inventory based on 2015 for the point sources of category A (public power) and the sum of sectors from area sources at the four grid pixels where the power plants are located.

CAMS NOx Emission (Tonnes/year)	Ag. Dimitrios	Kardia	Amyntaio	Meliti
Point sources (Public power)	11000	8060	3190	694
Rest emitting sources	181	125	141	127

2.3. *The S5P/TROPOMI satellite observations*

The Sentinel-5 Precursor (S5P) satellite, launched in October 2017, carries the TROPOsperic Monitoring Instrument (TROPOMI), a passive nadir-viewing spectrometer. TROPOMI provides measurements of the atmospheric composition at an unprecedented spatial resolution of 7×3.5km^2 at nadir (5.5×3.5km^2 since 6 August 2019) with near global coverage in one day. S5P is in an orbit at an altitude of 817 km with an overpass of around 13:30 local solar time [22]. The TROPOMI NO_2 retrieval algorithm is based on the DOMINO NO_2 retrieval that is used on its predecessor instrument OMI/Aura [23] and is developed by the Royal Netherlands Meteorological Institute (KNMI), described in the product Algorithm Theoretical Basis Document (ATBD, [24]). Validation studies indicated that TROPOMI systematically underestimates the NO_2 columns at extremely polluted regions reaching up to biases of 30% [25–27], while it overestimates low NO_2 columns [28,29]. Recent studies [25,28] suggest that the use of high-resolution *a priori* profiles from regional models (e.g. from the regional CAMS ensemble) will increase the retrieved tropospheric column by 10-30% over polluted locations with high emissions, explaining part of the bias. Notably, when model outputs are compared with TROPOMI observations using the averaging kernels (as is done in this paper), the a-priori profile shape used in the retrieval does not influence the relative comparison. Other uncertainties are related to the surface albedo climatology, and cloud (aerosol) retrievals, and may be responsible for remaining biases of order 10-20%. The TROPOMI NO_2 data are routinely validated by comparisons to ground-based reference measurements by the Mission Performance Center Validation Data Analysis Facility (VDAF, http://mpc-vdaf.tropomi.eu).

The NO_2 S5P/TROPOMI observations used for the assimilation in the present study are obtained via the Copernicus Open Data Access Hub (https://s5phub.copernicus.eu/). The level 2 reprocessed data, RPRO, v01.02 for summer 2018, while for 2019 the offline data (OFFL v1.03) are used. The data are filtered for a quality assurance value higher than 0.75 to ensure mostly cloud-free pixels, as recommended by the Product User Manual (PUM, [30]).

2.4. *Ensemble Kalman Filter around LOTOS-EUROS CTM*

As mentioned above, the emissions used in the simulation model form a source of uncertainty. In the context of the data assimilation algorithm, the uncertain emissions are modelled according to:

$$e[k] = e_b[k]\delta e[k] \quad (1)$$

where $e_b[k]$ are the *a priori* emissions at time k and $\delta e[k]$ is a stochastic emission correction factor. In order to specify a smooth uncertainty as described in [31], the emission correction factor follows a structure of a colored noise process instead of a white noise that would be uncorrelated in time [32]. The colored noise has zero mean and standard deviation σ and is implemented by:

$$\delta e[k+1] = \alpha[\kappa]\delta e[k] + \sqrt{1-\alpha^2}\sigma w[k] \tag{2}$$

In here $w[k]$ is a white noise vector uncorrelated in time with zero mean and unity standard deviation. Factor $\alpha \in [0,1]$ is a time correlation parameter that is used to describe the temporal variation following:

$$a = \exp\left(-\frac{|t[k] - t[k-1]|}{\tau}\right) \tag{3}$$

where τ is a temporal length scale, and $t[k] - t[k-1]$ is the time step used. The choice of a suitable value for τ is described in Appendix A.

In the Ensemble Kalman Filter, the model uncertainty is represented by an ensemble of state vectors. Here, an augmented state vector is used, containing both the concentrations (*c)* and the emissions correction factors (δe). In this way, the assimilated states also provide an estimate of the emission correction. The state vectors are propagated in time using the LOTOS-EUROS model, M, and the colored noise model:

$$\begin{bmatrix} c[k] \\ \delta e[k] \end{bmatrix} = \begin{bmatrix} M(c[k-1], \delta e[k-1]) \\ \delta e[k-1] \times \alpha[k-1] \end{bmatrix} + \begin{bmatrix} 0 \\ \sqrt{1-\alpha^2}\sigma \end{bmatrix} w[k] \tag{4}$$

The ensemble is propagated by the model until observations, y[k], become available. The observations are then used to analyze the ensemble such that the remain distribution is in agreement with the observations. The simulation of the observation by a state x is described by:

$$y[k] = H[k]x[k] + v[k] \quad , \quad v[k] \sim N(0, R) \tag{8}$$

In here, H is the nonlinear observation operator used to transform the background states from the model space to the observational space; for the satellite NO_2 observations this contains the averaging kernel of the satellite product. Vector $v[k]$ is the observation representation error with zero mean and covariance R. The covariance R is defined by the retrieval errors provided by the observational data.

For the analysis the Local Ensemble Transform Kalman Filter-LETKF algorithm is used [33]. The algorithm analyses the state per grid cell. First, all the observations and the corresponding ensemble simulations within a certain distance from the grid cell are collected. This distance depends on the selection of a length-scale called localization radius, ρ. Observations within a distance of 3.5ρ from the grid cell are selected and weighted relative to the inverse of their distance from the grid cell and based on the ρ. These are then used to update the ensemble in the grid cell. For small length-scales, the analysis only changes the ensemble in the grid cells with or close to observations, while using a longer length-scale more observations are used for the analysis of a single grid cell. In this way, the observations that affect the point analysis in each time step depend on the length-scale. In this study, we defined a localization radius equal to 14 km following sensitivity experiments described in Appendix A. The required ensemble size depends (among others) on the choices for ρ and τ, the sensitivity experiments suggested that a small ensemble size of only 12 members is sufficient for the chosen configuration.

2.5. In situ NO_2 measurements

For the validation of the simulations, as well as for choosing the optimal configuration of the assimilation system over the studied region, hourly in situ surface NO_2 measurements from air quality stations in the region have been acquired for the summers of

2018 and 2019 (Dr Evagelopoulos V., University of Western Macedonia, private communication). The location of the stations is shown in **Figure 1**. Time series of NO_2 measurements from the Koilada station [21.9307 E, 40.3557 N], located in the grid cell of the biggest power plant of the region, are shown in **Figure 4**. The NO_2 mean concentration in summer 2018 is 6.22±3.93 μg/m³, while in 2019 it is decreased to a mean value of 3.39±2.74 μg/m³. Time series at the Florina station [21.4103, 40.7821], which is in the town of Florina, and the Amyntaio station [21.6818, 40.6789], which is ~8 km from the Amyntaio power plant and ~1.5 km from the town of Amyntaio, are available as supplementary material in **Figure S2** and **Figure S3.**

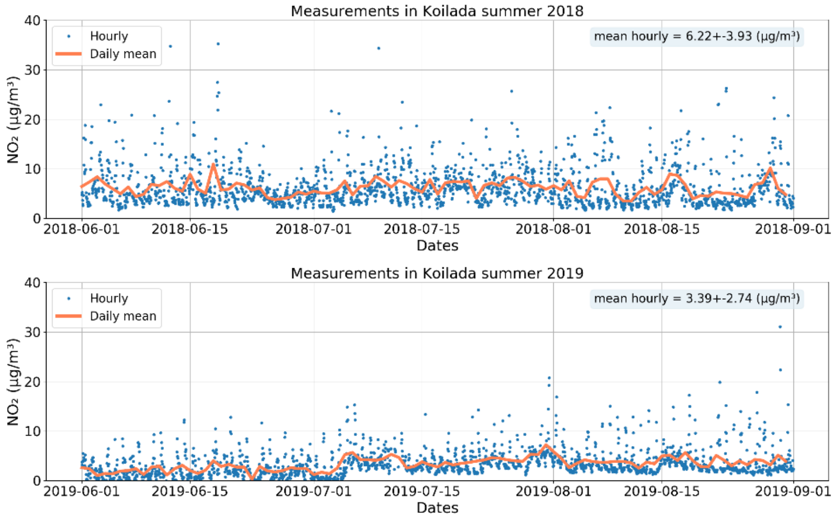

Figure 4. Time series of NO_2 hourly measurements (blue dots) at the station of Koilada and the daily mean NO_2 (orange line) for the summer of 2018 (top) and 2019 (bottom).

3. Results

3.1. LOTOS-EUROS NO_2 simulations and S5P/TROPOMI observations

The S5P/TROPOMI tropospheric NO_2 observations are regridded onto the model grid (0.10°×0.05°) using a standard area-weighted averaging method. The observations are weighted depending on their distance from each grid point and the relative average is then calculated. Simulations of the regridded observations are then obtained by application of the averaging kernels (AK) of the satellite product to the LOTOS-EUROS concentrations. The simulated concentrations are first mapped to the retrieval's a-priori layers to make the comparison between them feasible; the model top at 200 hPa is exactly sufficient to cover the TROPOMI tropospheric column. In this way, the vertical sensitivity of the satellite instrument is taken into account in the comparisons between the model and the observations. The averaging kernels are applied to the model output at the closest time of the satellite overpass, which is on average between 11:00 to 12:00 UTC.

For summer 2019, the averaged NO_2 tropospheric columns as observed by S5P/TROPOMI are shown in **Figure 5 (a).** The corresponding model NO_2 values after the averaging kernel of the satellite retrieval are applied are shown in **Figure 5 (b).** The same figures for the summer of 2018 are shown in **Figure S4.** The number of available daily satellite observations over the two larger power plants is lower in 2018 compared to 2019, with ~53 and ~70 pixels, respectively. The retrievals and the simulations show similar spatial distributions, with higher values around the two largest power plants, Ag. Dimitrios and Kardia. However, large discrepancies in the absolute values of NO_2 are found around the larger power plants where LOTOS-EUROS overestimates NO_2 in comparison with S5P/TROPOMI observations. During summer 2019, LOTOS-EUROS simulates an average column of about 9×10^{15} molec.cm^{-2} while TROPOMI observes about 2×10^{15} molec.cm^{-2} over the same grid cell where Ag. Dimitrios is located (**Table 2**). A high model bias is also found over the power plant of Kardia (bias of 4.5×10^{15} molec.cm^{-2}), whereas the discrepancy is negligible over the small Meliti power plant. The column simulations are lower for summer 2018 than for summer 2019 (**Figure 6**) even though the *a priori* emissions used are the same. This can be attributed to the different meteorological conditions taking place that affect the NO_2 levels together with the different number of daily available satellite observations.

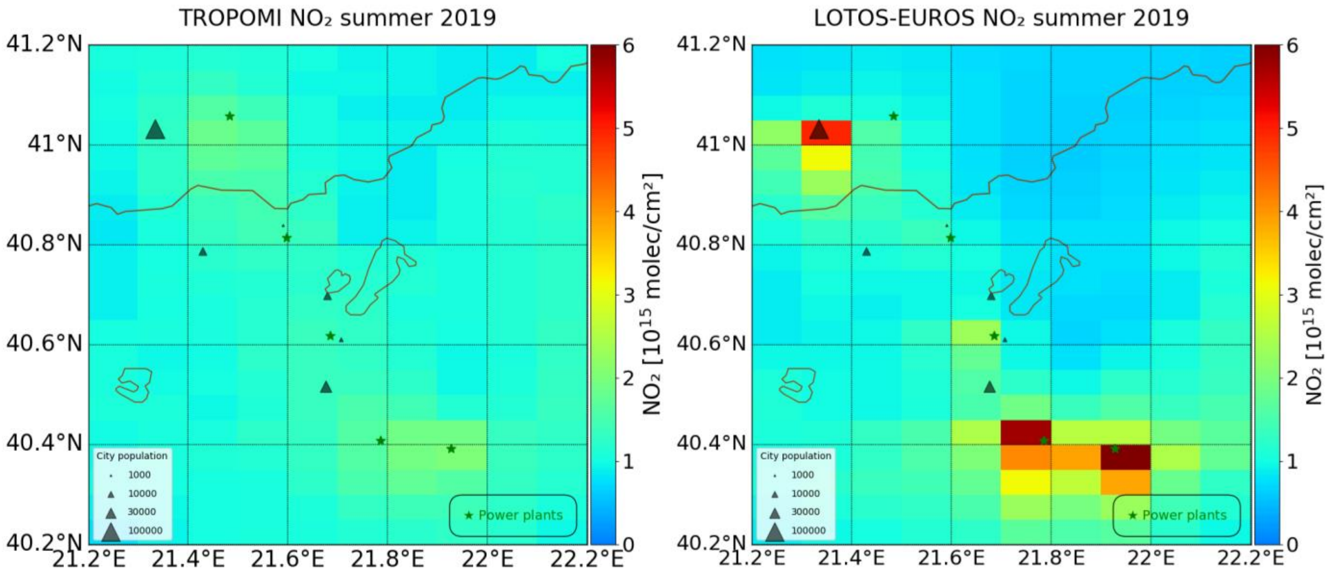

Figure 5. (a) Seasonal averaged NO_2 tropospheric columns in summer 2019 from S5P/TROPOMI retrieval; **(b)** LOTOS-EUROS NO_2 tropospheric simulation in summer 2019 after the averaging kernels of the satellite product are applied.

Table 2. Statistics (mean values, standard deviation and bias) of the NO_2 tropospheric column observed by S5P/TROPOMI and the simulations of LOTOS-EUROS after the averaging kernel is applied in 10^{15} molecules/cm^2 for summer 2018 and 2019 over the 4 grid cells where the power plants are located.

Power plants	2018			2019		
	TROPOMI	**LOTOS-EUROS**	**Bias**	**TROPOMI**	**LOTOS-EUROS**	**Bias**
Ag. Dimitrios	3.70±2.42	7.29±5.14	3.59	2.11±1.43	8.97±6.17	6.86
Kardia	3.20±2.51	4.75±3.83	1.55	1.64±0.67	6.13±4.31	4.50
Amyntaio	2.13±1.20	2.88±1.90	0.75	1.37±0.53	2.38±0.93	1.01
Meliti	1.61±0.61	1.33±0.50	-0.28	1.46±0.47	1.40±0.96	-0.06

3.2. *Updated assimilated NOx emissions*

The choice for localization radius ρ and the temporal parameter τ is crucial for the performance of the assimilation system, and are studied with different sensitivity tests shown in Appendix A. The selected localization radius is 14 km and the temporal parameter is 7 days, since these values showed the best performance during the assimilation. A rather small ensemble size of 12 members was sufficient to obtain stable results, as also found in other studies using the same system [34].

 doi:10.20944/preprints202106.0143.v1

After assimilation, the LOTOS-EUROS columns are decreased as expected (**Figure 6**). The biases between the assimilated columns and the observations over the four power plants are lower than 0.6 molec.cm^{-2} for both 2018 and 2019. In the grid cell where Ag. Dimitrios is located, the average NO_2 column in summer 2019 (2018) in the assimilated run is about 2.4×10^{15} molec.cm^{-2} (4×10^{15} molec.cm^{-2}), while TROPOMI observes about 2×10^{15} molec.cm^{-2} (3.70×10^{15} molec.cm^{-2}) during the same period.

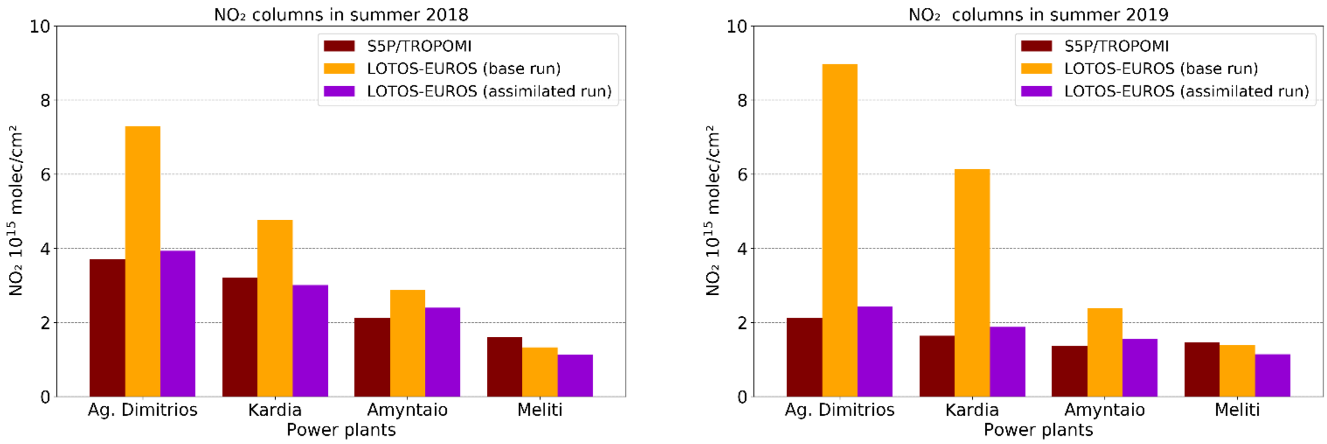

Figure 6. Mean tropospheric NO_2 columns: observed by TROPOMI instrument (brown bars), simulated by LOTOS-EUROS (orange bars) and assimilated with S5P/TROPOMI (purple bars) for (a) summer 2018 and ; **(b)** summer 2019.

The *a priori* and *a posteriori* NO_x emissions during the summer of 2019 over the four grid pixels where the power plants are located are shown in **Figure 7** (**Figure S5** for 2018). The TROPOMI-based emissions are in general lower relative to the *a priori* emissions which refer to year 2015. The updated emissions over the power plant of Ag. Dimitrios are 38% and 63% lower than a-priori emissions in 2018 and 2019, respectively. Similarly, over the Kardia power plant the emissions in 2018 were decreased by 27% in 2018 and by 63% in 2019. In 2018, over the Amyntaio plant negligible emission changes were inferred whereas in 2019 the a posteriori emissions are 37% lower than the *a priori*. Finally, over the smallest plant of Meliti no important differences are found, and only a small decrease of 11% is found for 2018 (**Table 3**).

Preprints (www.preprints.org) | NOT PEER-REVIEWED | Posted: 4 June 2021 doi:10.20944/preprints202106.0143.v1

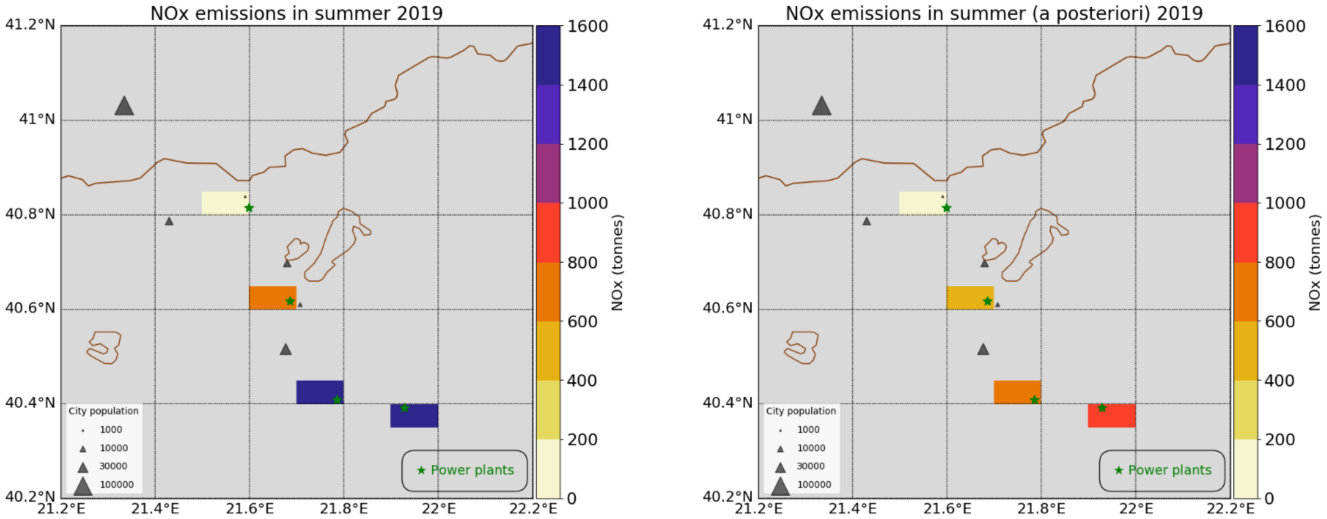

Figure 7. Aggregated NO_x emissions at the four pixels in Northwest Greece in summer 2019 (a) *a priori* and (b) assimilated *a posteriori*.

Table 3. Relative differences between *a posteriori* emissions estimated in summer 2018 and 2019 and *a-priori* emissions used for the simulations over the four grid-pixels.

Relative differences	Ag. Dimitrios	Kardia	Amyntaio	Meliti
2018 – 2015	-38%	-27%	-1%	-11%
2019 – 2015	-63%	-63%	-37%	-1%

The daily time series of NO_x emissions over the grid cell where Ag. Dimitrios is located is shown in top of **Figure 8** for 2018 (left) and 2019 (right). A clear weekly profile is visible in the *a priori* emissions (orange line) representing the lower NO_x emissions assumed during the weekends and stable emissions during the week. It is also shown that during July the emissions are slightly lower than in June and August (~-1% and ~-8% respectively). However, the *a posteriori* emissions (purple line) do not follow these profiles. In 2018 the estimated emissions are found to strongly decrease in August by around 40% and 30% compared to June and July respectively while in 2019 they remain low throughout the period of summer and decrease by 28% in August compared to June and July. A clear day-of-the week profile is not visible either. A large τ selection is reasonable for the case of the power plants, since a large day-to-day emission variation is not expected, but rather a relatively constant bias during all months. No changes in the diurnal variability are found (**bottom of Figure 8)**, as could be expected, since only one satellite measurement per day is available. However the *a posteriori* diurnal emissions in 2019 are much lower than the inferred emissions in 2018 and are decreased by more than 60% compared to the *a priori* emissions.

Preprints (www.preprints.org) | NOT PEER-REVIEWED | Posted: 4 June 2021 doi:10.20944/preprints202106.0143.v1

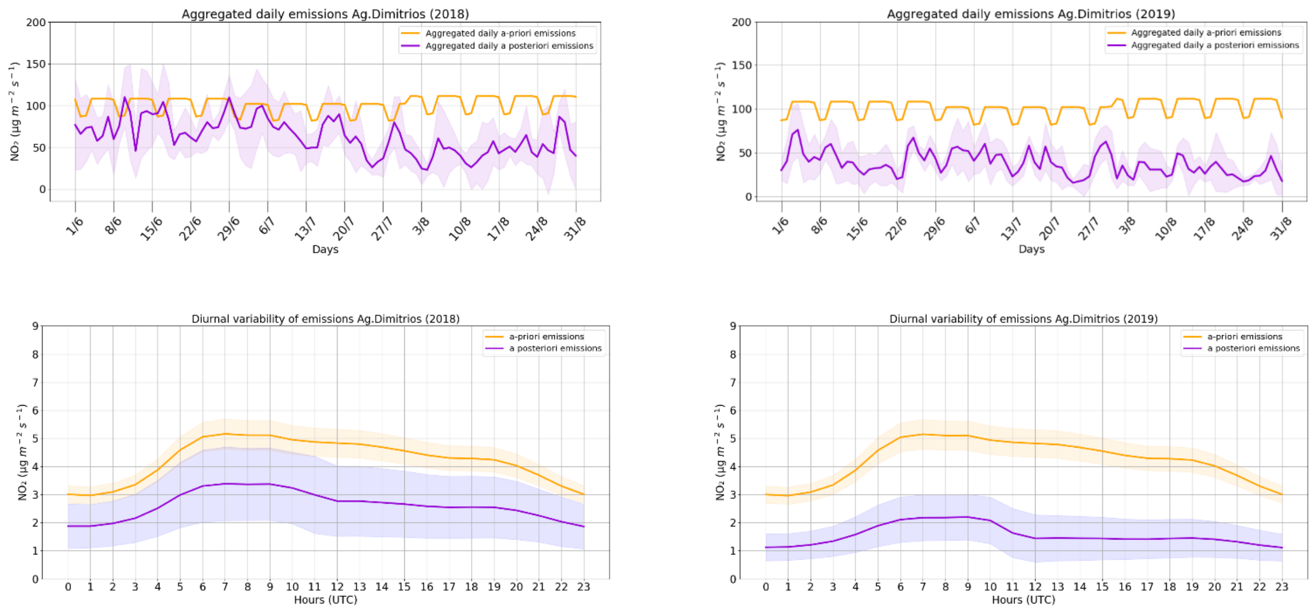

Figure 8. Top: Aggregated daily NO_x *a-priori* emissions (orange line) and *a posteriori* NOx emissions (purple line) together with the propagated uncertainty of the emission correction factors (shaded purple area) derived from S5P/TROPOMI assimilation over the grid pixel where the Ag. Dimitrios power plant is located (a) for summer 2018 and ; (b) summer 2019. **Bottom**: Diurnal variability of the emissions over the same grid pixel and periods.

The annual amount of NO_x emitted from the power plants for the years 2018 and 2019 are obtained from the E-PRTR repository and compared to the estimated *a posteriori* emissions. To allow comparison with the yearly estimates of E-PRTR, we extrapolate the summertime *a posteriori* emissions to annual totals estimates assuming that there is no seasonal variability in the power plants emissions. The relative differences of the E-PRTR reported from 2015 to 2018 and 2019 are shown in **Figure 9**. The NO_x emissions of the three larger power plants show a good overall agreement in both 2018 and 2019. The changes reported by E-PRTR in 2019 are -62% and -72% for Ag. Dimitrios and Kardia power plants respectively, while the estimated changes are -70% for both power plants. In 2018, the changes reported by E-PRTR for Ag. Dimitrios and Kardia power plants are -35% and -38%, respectively, while the estimated changes in the *a posteriori* emissions are -50% and -42% respectively, showing a good agreement in this case as well. The case of Meliti power plant is less representative of the grid cell where it is located, since as already discussed before (in section 2.2) there are more emission sources in the region and the power plant has a small capacity (~290 MW). Moreover, in **Figure 5** a first indication of transboundary pollution was evident. To further prove this, windroses are plotted using the ECMWF wind components used for the simulations, for the hour closer to the TROPOMI overpass over the area (~12:00 UTC). Figure S7 and S8 show the wind direction and speed over the pixels of the power plant and the city of Bitola, in the neighboring country (Republic of North Macedonia), for the summer of 2018 and 2019 respectively. The dominant winds for both seasons are North and Northeast. Furthermore, Figure S9 shows that the dominant winds over Meliti power plant are of a Northwest direction for both 2018 and 2019. According to these findings, it is safe to assume that NO_x from Bitola is affecting the Meliti power plant near the border of the two countries.

Preprints (www.preprints.org) | NOT PEER-REVIEWED | Posted: 4 June 2021 doi:10.20944/preprints202106.0143.v1

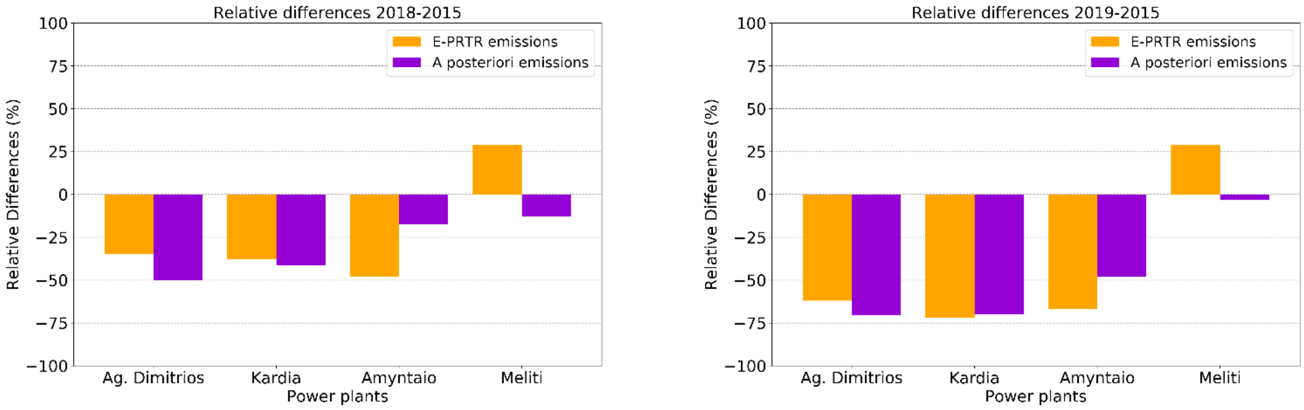

Figure 9. Relative differences of E-PRTR annual emissions of the power plants (orange bars) and relative differences between the assimilated annual emissions of the grid pixels as estimated (purple bars) (a) for 2018 and (b) 2019, both with respect to E-PRTR 2015 reported emissions.

3.3. *Validation of the a posteriori NOx simulations*

3.3.1. In-situ measurements

In order to validate the *a posteriori* NO_x simulations, surface NO_2 concentrations simulated using the *a priori* emissions (base run) and the TROPOMI-based emissions (assimilated run) are compared with hourly in situ NO_2 measurements. In **Figure 10** the mean summer surface NO_2 as simulated by the base run (left) and the assimilated run (right) are shown together with the mean summer NO_2 values of the in situ stations in 2018 (**top**) and 2019 (**bottom**), depicted as colored circles. The assimilated NO_2 concentrations are reduced over the whole region and especially around the power plants of Ag. Dimitrios and Kardia compared to the base run (**Figure 10**).

The NO_2 measurements of Koilada station, which is affected by the largest power plant in the area, are lower in 2019 (3.39±2.74 μg/m³) compared to 2018 (6.22±3.93 μg/m³). For both years the NO_2 measurements are much lower than the base run results (bias of 10.52 μg/m³ in 2019 and 8.46 μg/m³ in 2018), while the assimilated run succeeds in reducing the bias (biases of 2.0 μg/m³ in 2019and 2.8 μg/m³ in 2018) (**Table S1** and **Table 4**). Furthermore, the diurnal variability of the air quality observations in Koilada (**Figure 11**, upper) is better represented by the assimilated runs since the concentrations are much closer to the measurements, as is also found for the morning diurnal simulations at the Florina air quality station (**Figure 11**, bottom).

Similarly, surface NO_2 concentrations measured from the Amyntaio air quality station, which is affected by the neighboring town and power plant, are lower than the base run results (bias 3.49 μg/m³ in 2019 and 1.13 μg/m³ in 2018), while the biases are reduced when compared with the assimilated concentrations (bias 1.73 μg/m³ and 0.85 μg/m³ in 2019 and 2018 respectively). It is also worth mentioning that the NO_2 measurements in 2019 are lower than in 2018 in this case as well (4.00±2.25 μg/m³ and 6.37±3.82 μg/m³ respectively).

Surface NO_2 levels measured in Meliti station are high in 2019 (8.18±6.46 μg/m³) and 2018 (10.93±11.05 μg/m³) and the model underestimates the NO_2 levels both before and after assimilation. This is possibly due to possible transboundary pollution from the Bitola power plant, already discussed in literature [35]. To state that, as already discussed in Section 2.5, the prevailing winds of N-NW direction, appear to transport pollution

Preprints (www.preprints.org) | NOT PEER-REVIEWED | Posted: 4 June 2021 doi:10.20944/preprints202106.0143.v1

from the power plant and the city of Bitola in the Rebublic of North Macedonia to North Greece.

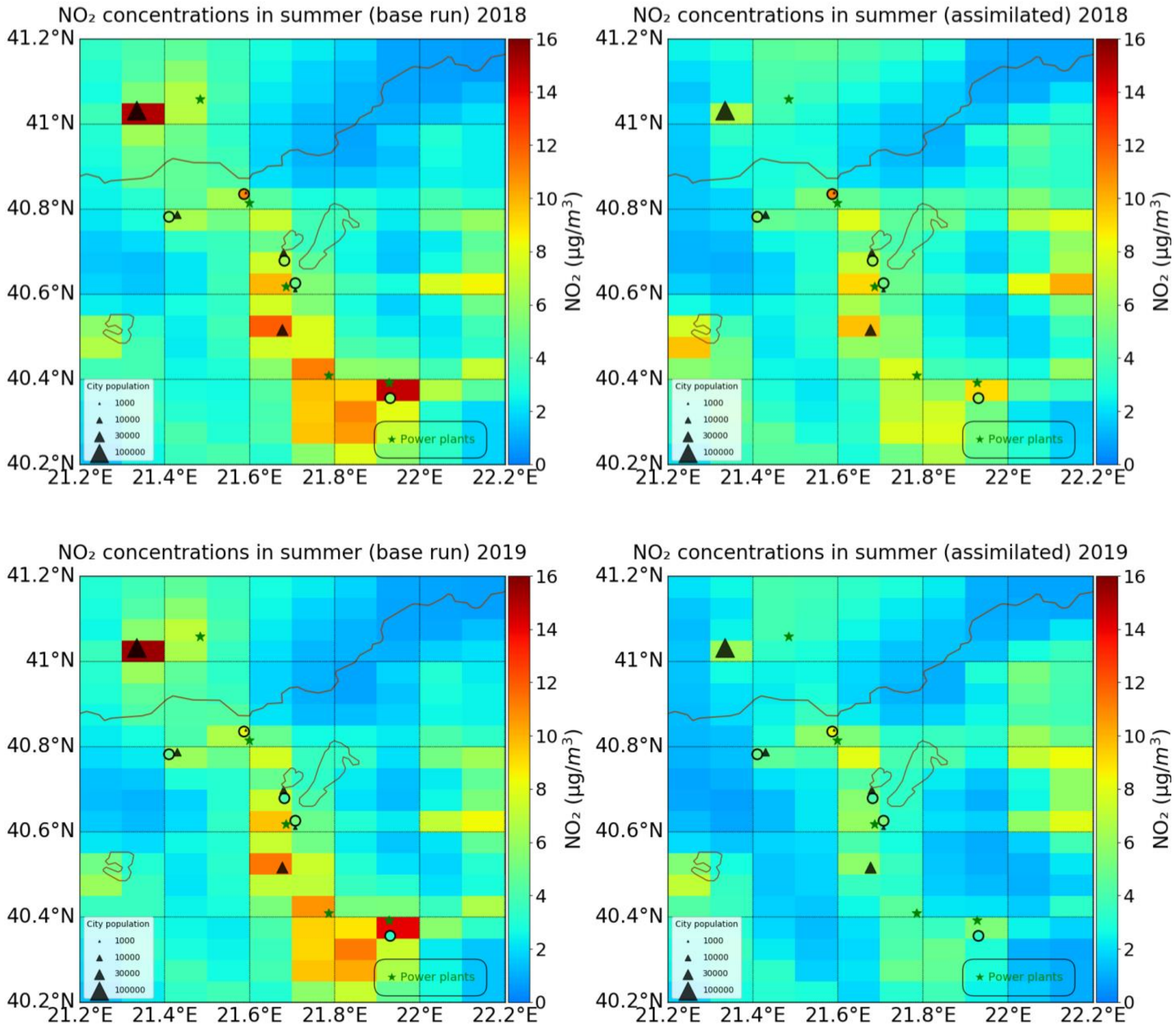

Figure 10. LOTOS-EUROS surface simulations compared with in situ measurements, shown as coloured circles. (a) base run for summer 2018; **(b)** assimilated run for summer 2018. **(c)** as (a) for summer 2019. **(d)** as (b) for summer 2019. The color of the circles indicates the average summer-time level of the in situ measurements.

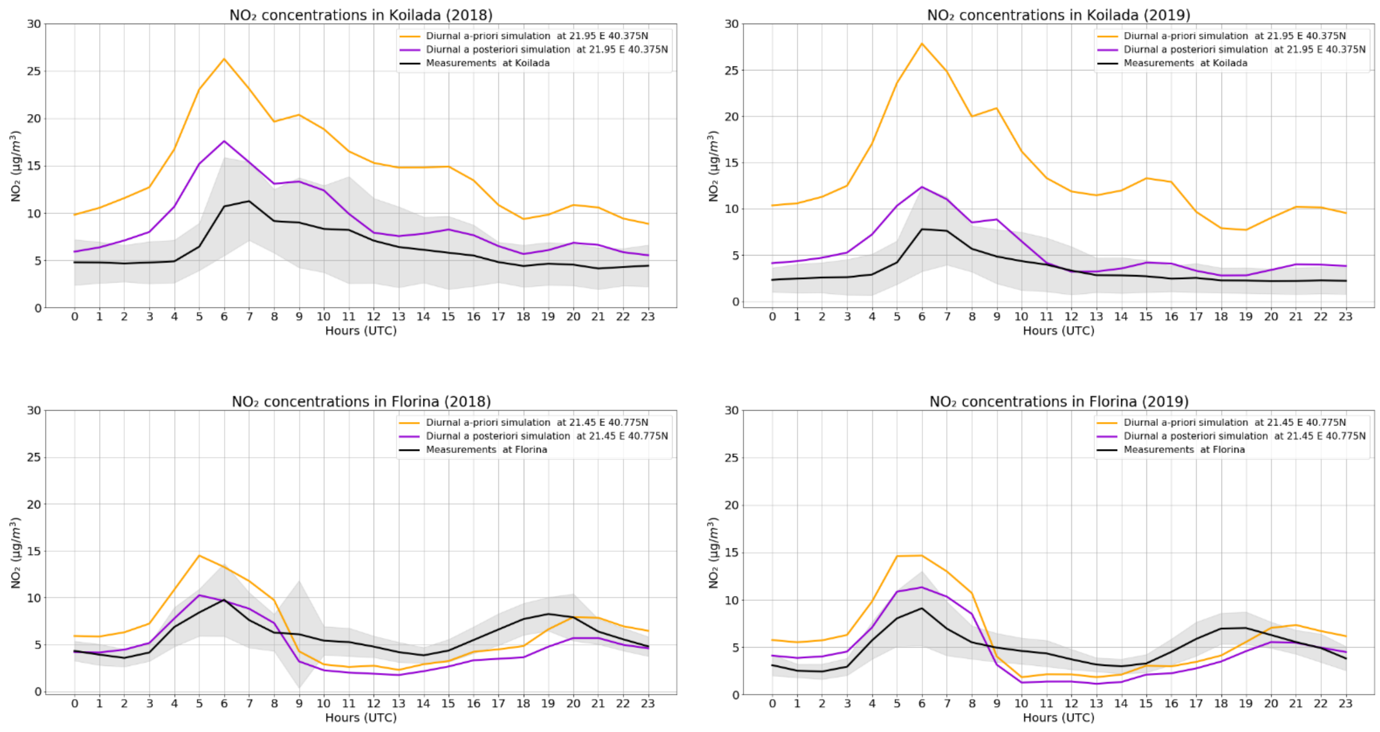

Figure 11. (a) Diurnal variability of NO_2 surface concentrations as simulated by the model using the *a-priori* emissions (orange lines) and the *a posteriori* emissions from S5P/TROPOMI assimilation (purple lines) and in-situ measurements (black lines) of the stations of Koilada (top) and Florina (bottom) in summer 2018; **(b)** same as **(a)** for 2019.

Table 4. Statistics of the comparison of LOTOS-EUROS surface simulations in the base and assimilated runs with surface measurements in summer **2019.** P.P. refers to power plant.

Air Quality stations	Emission sources	Seasonal mean (μg/m³) ±std			Bias (μg/m³)	
		Measurements	**Base run**	**Assimilated**	**Base run**	**Assimilated**
Koilada	P.P. Ag. Dimitrios	3.39±2.74	13.92±10.18	5.39±4.65	10.52	**2.00**
Filotas	Town of Filotas/ P.P. Amyntaio	5.38±3.52	4.91±4.46	3.12±3.12	-0.47	-2.26
Amyntaio	Town of Amyntaio/ P.P. Amyntaio	4.00±2.25	7.49±7.57	5.73±6.35	3.49	**1.73**
Meliti	Town of Meliti/P.P. Meliti/ P.P. Bitola	8.18±6.46	6.55±6.23	5.84±6.49	-1.63	-2.34
Florina	Town of Florina	4.93±2.45	6.10±6.35	4.57±5.65	1.17	**-0.35**

3.3.2. Energy production of the power plants

In order to further evaluate the updated *a posteriori* NO_x emissions, the reported monthly energy production data per power station are examined. The aforementioned data are available publicly through reports of the Day-ahead Scheduling Archive for Greece and are available online by the Energy Exchange Group-EnEx (www.enexgroup.gr). Monthly as well as yearly energy production data for the four power plants are extracted for years 2015, 2018 and 2019.

The total energy production per power plant for the summer period studied in years 2015, 2018 and 2019 is shown **Figure 12 (a)** together with the *a priori* emissions in summer based in 2015 CAMS-REG emission inventory and the assimilated NO_x emissions for 2018 and 2019 in **Figure 12 (b).** The energy production of the Ag. Dimitrios, Kardia and Amyntaio power plants decreases in 2018 and 2019 compared to 2015. These reductions are in accordance with the reductions found in the corresponding *a posteriori* NO_x emissions (**Figure 12 (b)**). It is also shown that energy production and NO_x emissions in 2019 are even lower than in 2018. The relative differences between the *a priori* and *a posteriori* emissions directly compared to the relative differences between the power plant energy productions are shown in **Figure 12** for 2018-2015 and 2019-2015. Over the two larger power plants (Ag. Dimitrios and Kardia), the changes in energy and emissions are consistent for both 2018 and 2019. Larger decreases are found for both energy and emissions in 2019 compared to 2018 as well. In the case of the Meliti power plant, the emissions remain nearly the same, despite the fact that the energy production in 2019 is twice lower than in 2015 and 2018. Overall, the emission reduction is even more pronounced in 2019 compared to 2015 at the three largest power plants of Ag. Dimitrios, Kardia and Amyntaio and this is further confirmed by the reduction of the energy production in the same year that reaches at least 50%.

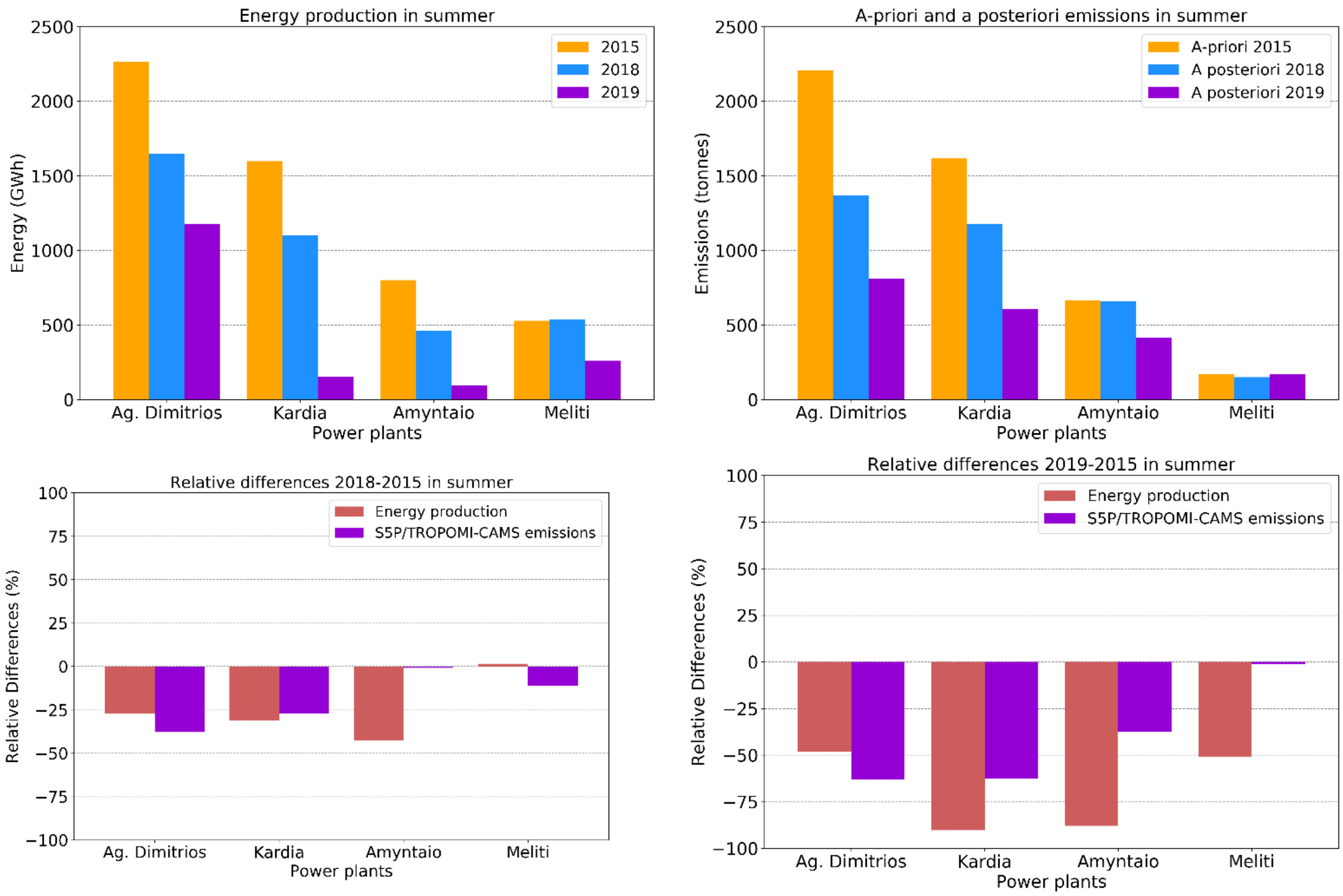

Figure 12. Top: (a) Bar plots of the energy production of the four power plants reported for the summer of 2015 (orange bars), 2018 (blue bars) and 2019 (purple bars); **(b)** Bar plots of the *a-priori* 2015 CAMS-REG emissions in summer (orange bars) and *a posteriori* emissions in summer 2018 (blue bars) and 2019 (violet bars) over the grid-pixels where the four power plants are located. **Bottom:** Relative differences between seasonal *a posteriori* and *a priori* emissions (purple bars) in the four grid pixels and energy production (red bars) of the four power plants between (a) 2018 and 2015; (b) 2019 and 2015.

4. 4. Conclusions

In this work, an advanced data assimilation system is used to estimate the NO_x emission changes at four lignite power plants operating in Northwest Greece. The operation

Preprints (www.preprints.org) | NOT PEER-REVIEWED | Posted: 4 June 2021 doi:10.20944/preprints202106.0143.v1

of the four power plants; Ag. Dimitrios, Kardia, Amyntaio and Meliti (sorted by the largest reported capacity), is subject to massive changes due to Greece's target of reducing the total greenhouse gases by 2023. An ensemble Kalman filter operating around the LOTOS-EUROS CTM is employed to estimate the NO_x surface emissions with a resolution of 0.1° in longitude and 0.05° in latitude using S5P/TROPOMI NO_2 column retrievals. The *a priori* anthropogenic emissions are based on reports for 2015 and are obtained from Copernicus Atmosphere Monitoring Service-Regional European emissions (CAMS-REG) version 4.2. Our main conclusions can be summarized below.

- The *a posteriori* emissions estimated for the two largest power plants of **Ag. Dimitrios and Kardia are much lower in 2019 than in 2018**. In 2019 the estimated emissions are decreased by more than 60% compared to the *a priori* emissions, while in 2018 are reduced by around 33%, relative to the 2015 inventory**.** The *a posteriori* emissions over the **Amyntaio** power plant show no changes in 2018, but are strongly reduced in 2019, by ~37%.
- The annual emissions reported **by E-PRTR agree well with the calculated *a posteriori* annual NO_x emissions** over the two largest power plants. The *a posteriori* annual emission changes estimated over the two larger power plants in 2018 compared to the *a priori* 2015 emissions, are ~ -40% to -50%, whereas the changes for 2019 are ~ -70% for both power plants. The changes in the annual emissions of 2019 (2018) compared to 2015 reported **by the E-PRTR emissions database** over Ag. Dimitrios and Kardia are -62% and -72% respectively (-35% and -38% respectively)
- **Stronger decreases in the energy production** are reported for the **summer** period **of 2019 compared to summer 2018** as well, in line with the estimated emission reduction. The energy production of Ag. Dimitrios power plant decreased by around 50% in 2019 compared to 2015, while in Kardia and Amyntaio by 90% for summer 2019. In summer 2018 the energy production in the three larger power plants decreased by around 30-45%.
- NO_2 measurements from air quality stations **of Koilada and Amyntaio,** which are directly affected by pollution from the power plants of Ag. Dimitrios and Amyntaio, respectively, show **improved agreement** with the assimilated NO_2 simulations compared to the base run which is based on the 2015 CAMS *a priori* emissions. The bias in the station of Koilada near the power plant of Ag. Dimitrios improves to 2 $\mu g/m^3$ (2.83 $\mu g/m^3$) from 10.5 $\mu g/m^3$ (8.46 $\mu g/m^3$) in 2019 (2018).
- The results for the **Meliti** power plant were found not to be representative of the grid cell where the plant is located due to presence of other emission sources affecting that grid cell. Furthermore, the dominant winds over the Bitola and Meliti power plants are Northerly for both summer 2018 and 2019, showing that pollution may flow from the neighboring country of Republic of North Macedonia to Northwest Greece.
- Overall, the method proposed here is appropriate in detecting emission trends of local large emittors, and could be valuable also for regions in the world where no up-to-date emission inventories are available.

Supplementary Materials: The following are available online at www.mdpi.com/xxx/s1, Figure S1: title, Table S1: title, Video S1: title.

Author Contributions: Conceptualization, Maria-Elissavet Koukouli and Dimitris Balis; Methodology, Ioanna Skoulidou and Maria-Elissavet Koukouli; Software, Ioanna Skoulidou and Arjo Segers; Supervision, Maria-Elissavet Koukouli and Dimitris Balis; Visualization, Ioanna Skoulidou; Writing – original draft, Ioanna Skoulidou and Maria-Elissavet Koukouli; Writing – review & editing, Maria-Elissavet Koukouli, Arjo Segers, Astrid Manders, Dimitris Balis, Trissevgeni Stavrakou, Jos van Geffen and Henk Eskes.

Funding: This research has been co-financed by the European Union (European Regional Development Fund) and Greek national funds through the Operational Program "Competitiveness, Entrepreneurship and Innovation" (NSRF 2014-2020) by the "Panhellenic Infrastructure for Atmospheric Composition and Climate Change" project (MIS 5021516) and well as the "Innovative system for Air Quality Monitoring and Forecasting" project [code T1EDK-01697, MIS 5031298), implemented under the Action "Reinforcement of the Research and Innovation" Infrastructure.

Data Availability Statement: The S5P/TROPOMI observations are publicly available from the Copernicus Open Access Hub (https://scihub.copernicus.eu/, ESA, 2021). The LOTOS-EUROS CTM simulations are available upon request. The air quality monitoring station data are available by personal communication with Dr Evagelopoulos V. by the University of Western Macedonia. The E-PRTR data are available via the website https://prtr.eea.europa.eu/. The energy production reports are available online by the Energy Exchange Group-EnEx (www.enexgroup.gr). The OMI QA4ECV NO_2 Essential Climate Variable (ECV) precursor products are obtained from www.temis.nl.

Acknowledgments: We acknowledge the usage of modified Copernicus Sentinel data (2019–2020). Results presented in this work have been produced using the Aristotle University of Thessaloniki (AUTh) high-performance computing infrastructure and resources. Ioanna Skoulidou, Maria-Elissavet Koukouli, and Dimitris Balis would like to acknowledge the support provided by the IT Center of the AUTh throughout the progress of this research work.

Conflicts of Interest: The authors declare no conflict of interest.

Appendix A

Since different parameters may affect the performance of the assimilation system, a series of sensitivity tests were conducted in order to select the optimal configuration for the present study. The experiments were performed for July 2019 and the NO_2 surface simulations from the base run, using the *a priori* NO_x emissions, and the distinct assimilation experimental runs, using the updated *a posteriori* NO_x emissions, are compared with hourly NO_2 in-situ measurements of the air quality station Koilada (**Table A1**). The in situ station Koilada is located at the same grid cell as the Ag. Dimitrios power plant, which is the pixel with the largest bias between the model predictions and the S5P/TROPOMI observations (**Table A1**).

The first parameter examined is the localization radius (ρ) described in 2.4. The observations that affect the grid cell analysis in each time step depend on the length scale, which means that the larger the length selected the more observations are used for the analysis of a single grid cell. According to [36] a localization procedure will prevent spurious correlations that may appear in the analysis due to the finite ensemble size selected. For the sensitivity tests, a temporal correlation parameter was set equal to 3 days and 5 different values of ρ were examined; ρ of 0, 5, 7, 14 and 20 km. The performance improves when the length is increased to 14 km and the bias decreases to 2.68 μg/m^3 (**Table A1**), compared to a bias of 12.21 μg/m^3 of the base run and 6.01 μg/m^3 when selecting ρ equal to 7 km. The bias does not improve significantly when the localization radius is further increased to 20 km (bias of 2.61 μg/m^3) (**Figure A1**). Moreover, since this study is focused in point sources of power plants and in the area around the stations no other significant NO_x sources are found, choosing a very large length may affect the results with observations of background values leading to an artificial NO_x decrease.

Preprints (www.preprints.org) | NOT PEER-REVIEWED | Posted: 4 June 2021 doi:10.20944/preprints202106.0143.v1

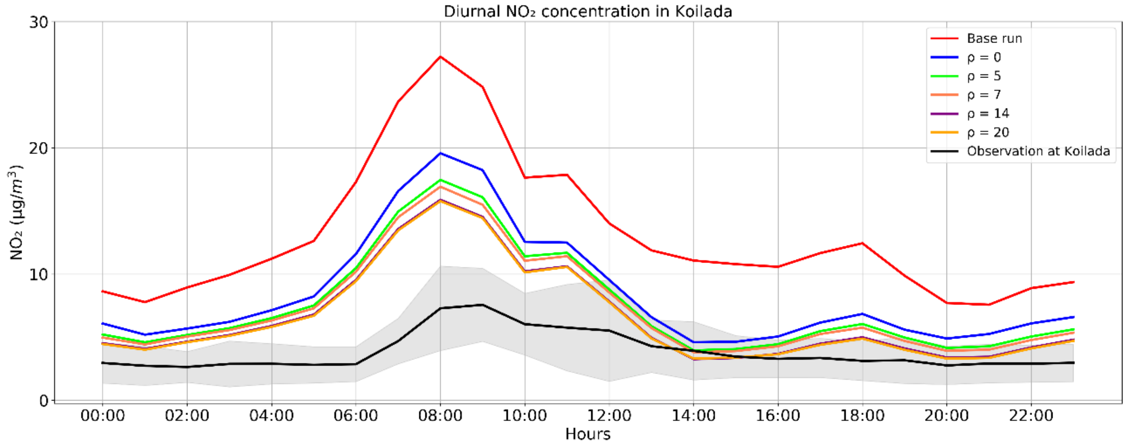

Figure A1. Diurnal cycle of the assimilated simulations of NO_2 in July 2019 from the sensitivity tests using ρ values of 0, 5, 7, 14 and 20 km in the grid pixel where Koilada air quality station and Ag. Dimitrios power plant are located. The black line denotes the in-situ measurement of Koilada station, with the associated standard deviation shown as a grey shaded area, while the red line the base run performed.

The second sensitivity experiment performed concerns the temporal correlation parameter (τ) described in section 2.4. Different values of τ are studied in the assimilation system; τ of 1, 3, 5 and 7 days, while the localization radius during the tests is fixed and equal to 14 km. The overestimations of the NO_2 simulations when compared to the in situ measurements reduces to a bias of 1.57 μg/m^3 (**Table A1**) when τ is equal to 7 days while when τ is small the NO_2 concentrations are less influenced and closer to the base run simulations (**Figure A2**). As a result the temporal parameter used for the assimilations is set to 7 days.

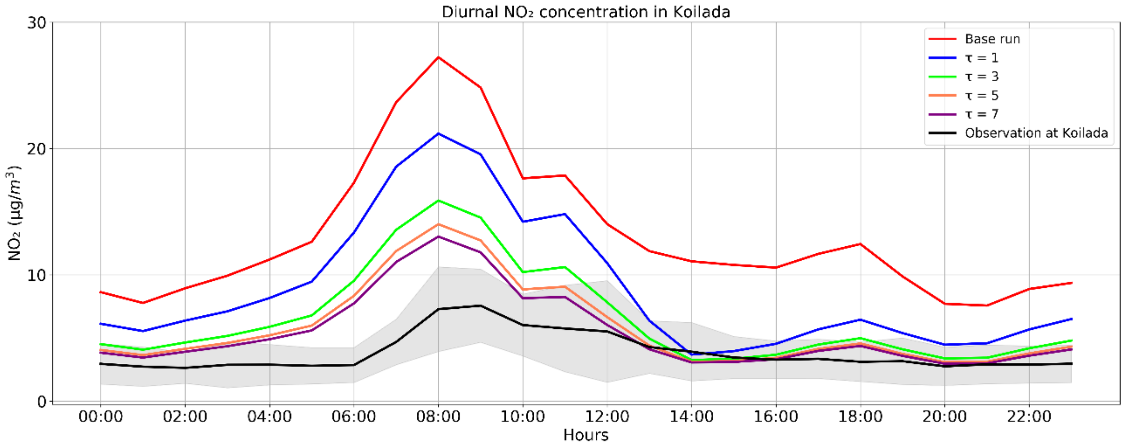

Figure A2 Diurnal cycle of the assimilated simulations of NO_2 in July 2019 from the sensitivity tests using τ values of 1, 3, 5 and 7 days [different coloured lines] in the grid pixel where Koilada air quality station and Ag. Dimitrios power plant are located. The black line denotes the in situ measurement of Koilada station, with the associated standard deviation shown as a grey shaded area, while the red line the base run performed.

Table A1. Performance of the EnKF system for different parameters; the localization radius (ρ) and the temporal correlation parameter (τ). Hourly in-situ measurements in the Koilada air quality station are compared with hourly surface simulations for July month. The statistics are given in μg/m^3.

Localization radius (ρ) in km			
Configuration	**Mean**	**Bias**	**RMSE**
Base run	13.05	9.17	12.21
ϱ = 0	8.37	4.49	7.40
ϱ = 5	7.46	3.58	6.36
ϱ = 7	7.20	3.31	6.01
ϱ = 14	6.56	2.68	5.31
ϱ = 20	6.49	2.61	5.23
Temporal correlation parameter (τ) in days			
Configuration	**Mean**	**Bias**	**RMSE**
Base run	13.05	9.17	12.21
τ = 1	8.83	4.95	8.04
τ = 3	6.56	2.68	5.31
τ = 5	5.82	1.94	4.52
τ = 7	5.46	1.57	4.18

References

1. Varshney, C.K.; Singh, A.P. Passive samplers for NOx monitoring: A critical review. *Environmentalist* **2003**, *23*, 127–136, doi:10.1023/A:1024883620408.
2. Miyazaki, K.; Eskes, H.J.; Sudo, K. Global NOx emission estimates derived from an assimilation of OMI tropospheric NO2 columns. *Atmos. Chem. Phys.* **2012**, *12*, 2263–2288, doi:10.5194/acp-12-2263-2012.
3. Streets, D.G.; Bond, T.C.; Carmichael, G.R.; Fernandes, S.D.; Fu, Q.; He, D.; Klimont, Z.; Nelson, S.M.; Tsai, N.Y.; Wang, M.Q.; et al. An inventory of gaseous and primary aerosol emissions in Asia in the year 2000. *J. Geophys. Res. Atmos.* **2003**, *108*, doi:10.1029/2002jd003093.
4. Müller, J.-F.; Stavrakou, T. Inversion of CO and NO2 emissions using the adjoint of the IMAGES model. *Atmos. Chem. Phys.* **2005**, *5*, 1157–1186, doi:10.5194/acp-5-1157-2005.
5. Castellanos, P.; Boersma, K.F. Reductions in nitrogen oxides over Europe driven by environmental policy and economic recession. *Sci. Rep.* **2012**, *2*, 1–7, doi:10.1038/srep00265.
6. Duncan, B.N.; Lamsal, L.N.; Thompson, A.M.; Yoshida, Y.; Lu, Z.; Streets, D.G.; Hurwitz, M.M.; Pickering, K.E. A space-based, high-resolution view of notable changes in urban NOx pollution around the world (2005–2014). *J. Geophys. Res.* **2016**, *121*, 976–996, doi:10.1002/2015JD024121.
7. Koukouli, M.E.; Skoulidou, I.; Karavias, A.; Parcharidis, I.; Balis, D.; Manders, A.; Segers, A.; Eskes, H.; Van Geffen, J. Sudden changes in nitrogen dioxide emissions over Greece due to lockdown after the outbreak of COVID-19. *Atmos. Chem. Phys.* **2021**, *21*, 1759–1774, doi:10.5194/acp-21-1759-2021.
8. Bauwens, M.; Compernolle, S.; Stavrakou, T.; Müller, J.F.; van Gent, J.; Eskes, H.; Levelt, P.F.; van der A, R.; Veefkind, J.P.; Vlietinck, J.; et al. Impact of Coronavirus Outbreak on NO2 Pollution Assessed Using TROPOMI and OMI Observations. *Geophys. Res. Lett.* **2020**, *47*, e2020GL087978, doi:10.1029/2020GL087978.
9. Wu, H.; Tang, X.; Wang, Z.; Wu, L.; Li, J.; Wang, W.; Yang, W.; Zhu, J. High-spatiotemporal-resolution inverse estimation of CO and NOx emission reductions during emission control periods with a modified ensemble Kalman filter. *Atmos. Environ.* **2020**, *236*, 117631, doi:10.1016/j.atmosenv.2020.117631.
10. Evensen, G. Sequential data assimilation with a nonlinear quasi-geostrophic model using Monte Carlo methods to forecast error statistics. *J. Geophys. Res.* **1994**, *99*, 10143–10162, doi:10.1029/94jc00572.

11. Triantafyllou, A.G. PM10 pollution episodes as a function of synoptic climatology in a mountainous industrial area. *Environ. Pollut.* **2001**, *112*, 491–500, doi:10.1016/S0269-7491(00)00131-7.
12. Levelt, P.F.; Joiner, J.; Tamminen, J.; Veefkind, J.P.; Bhartia, P.K.; Zweers, D.C.S.; Duncan, B.N.; Streets, D.G.; Eskes, H.; Van Der, R.A.; et al. The Ozone Monitoring Instrument: Overview of 14 years in space. *Atmos. Chem. Phys.* **2018**, *18*, 5699–5745, doi:10.5194/acp-18-5699-2018.
13. Manders, A.M.M.; Builtjes, P.J.H.; Curier, L.; Gon, H.A.C.D. Vander; Hendriks, C.; Jonkers, S.; Kranenburg, R.; Kuenen, J.J.P.; Segers, A.J.; Timmermans, R.M.A.; et al. Curriculum vitae of the LOTOS-EUROS (v2.0) chemistry transport model. *Geosci. Model Dev.* **2017**, *10*, 4145–4173, doi:10.5194/gmd-10-4145-2017.
14. Skoulidou, I.; Koukouli, M.-E.; Manders, A.; Segers, A.; Karagkiozidis, D.; Gratsea, M.; Balis, D.; Bais, A.; Gerasopoulos, E.; Stavrakou, T.; et al. Evaluation of the LOTOS-EUROS NO2 simulations using ground-based measurements and S5P/TROPOMI observations over Greece. *Atmos. Chem. Phys.* **2021**, *21*, 5269–5288.
15. Schaap, M.; Timmermans, R.M.A.; Roemer, M.; Boersen, G.A.C.; Builtjes, P.J.H.; Sauter, F.J.; Velders, G.J.M.; Beck, J.P. The LOTOS-EUROS model: Description, validation and latest developments. *Int. J. Environ. Pollut.* **2008**, *32*, 270–290, doi:10.1504/IJEP.2008.017106.
16. Fountoukis, C.; Nenes, A. ISORROPIA II: a computationally efficient thermodynamic equilibrium model for for K+–Ca2+–Mg2+–NH4+–Na+–SO42−–NO3−–Cl−–H2O aerosols. *Atmos. Chem. Phys* **2007**, *7*, 4639–4659, doi:10.5194/acp-7-4639-2007.
17. Flemming, J.; Inness, A.; Flentje, H.; Huijnen, V.; Moinat, P.; Schultz, M.G.; Stein, O. Coupling global chemistry transport models to ECMWF's integrated forecast system. *Geosci. Model Dev.* **2009**, *2*, 253–265, doi:10.5194/gmd-2-253-2009.
18. Granier, C.; Darras, S.; Denier Van Der Gon, H.; Jana, D.; Elguindi, N.; Bo, G.; Michael, G.; Marc, G.; Jalkanen, J.-P.; Kuenen, J. The Copernicus Atmosphere Monitoring Service global and regional emissions (April 2019 version). **2019**, 1–55, doi:10.24380/d0bn-kx16.
19. Beltman, J.B.; Hendriks, C.; Tum, M.; Schaap, M. The impact of large scale biomass production on ozone air pollution in Europe. *Atmos. Environ.* **2013**, *71*, 352–363, doi:10.1016/j.atmosenv.2013.02.019.
20. Novak, J.H.; Pierce, T.E. Natural emissions of oxidant precursors. *Water, Air, Soil Pollut.* **1993**, *67*, 57–77, doi:10.1007/BF00480814.
21. Kaiser, J.W.; Heil, A.; Andreae, M.O.; Benedetti, A.; Chubarova, N.; Jones, L.; Morcrette, J.J.; Razinger, M.; Schultz, M.G.; Suttie, M.; et al. Biomass burning emissions estimated with a global fire assimilation system based on observed fire radiative power. *Biogeosciences* **2012**, *9*, 527–554, doi:10.5194/bg-9-527-2012.
22. Veefkind, J.P.; Boersma, K.F.; Wang, J.; Kurosu, T.P.; Krotkov, N.; Chance, K.; Levelt, P.F. Global satellite analysis of the relation between aerosols and short-lived trace gases. *Atmos. Chem. Phys.* **2011**, *11*, 1255–1267, doi:10.5194/acp-11-1255-2011.
23. Boersma, K.F.; Eskes, H.J.; Dirksen, R.J.; Van Der A, R.J.; Veefkind, J.P.; Stammes, P.; Huijnen, V.; Kleipool, Q.L.; Sneep, M.; Claas, J.; et al. An improved tropospheric NO2 column retrieval algorithm for the Ozone Monitoring Instrument. *Atmos. Meas. Tech.* **2011**, *4*, 1905–1928, doi:10.5194/amt-4-1905-2011.
24. van Geffen, J.; Eskes, H.J.; Boersma, K.F.; Maasakkers, J.D.; Veefkind, J.P. *TROPOMI ATBD of the total and tropospheric NO2 data products, Report S5P-KNMI-L2-0005-RP, version 1.4.0*; KNMI, De Bilt, The Netherlands, available at: http://www.tropomi.eu/documents/atbd/, last access: 2 June 2021, 2019;
25. Dimitropoulou, E.; Hendrick, F.; Pinardi, G.; Friedrich, M.M.; Merlaud, A.; Tack, F.; De Longueville, H.; Fayt, C.; Hermans, C.; Laffineur, Q.; et al. Validation of TROPOMI tropospheric NO2 columns using dual-scan multi-axis differential optical absorption spectroscopy (MAX-DOAS) measurements in Uccle, Brussels. *Atmos. Meas. Tech.* **2020**, *13*, 5165–5191, doi:10.5194/amt-13-5165-2020.
26. Tack, F.; Merlaud, A.; Iordache, M.D.; Pinardi, G.; Dimitropoulou, E.; Eskes, H.; Bomans, B.; Veefkind, P.; Van Roozendael, M. Assessment of the TROPOMI tropospheric NO2 product based on airborne APEX observations. *Atmos. Meas. Tech.* **2021**, *14*, 615–646, doi:10.5194/amt-14-615-2021.

27. Verhoelst, T.; Compernolle, S.; Pinardi, G.; Lambert, J.C.; Eskes, H.J.; Eichmann, K.U.; Fjæraa, A.M.; Granville, J.; Niemeijer, S.; Cede, A.; et al. Ground-based validation of the Copernicus Sentinel-5P TROPOMI NO2 measurements with the NDACC ZSL-DOAS, MAX-DOAS and Pandonia global networks. *Atmos. Meas. Tech.* **2021**, *14*, 481–510, doi:10.5194/amt-14-481-2021.
28. Ialongo, I.; Virta, H.; Eskes, H.; Hovila, J.; Douros, J. Comparison of TROPOMI/Sentinel-5 Precursor NO2 observations with ground-based measurements in Helsinki. *Atmos. Meas. Tech.* **2020**, *13*, 205–218, doi:10.5194/amt-13-205-2020.
29. Zhao, X.; Griffin, D.; Fioletov, V.; McLinden, C.; Cede, A.; Tiefengraber, M.; Müller, M.; Bognar, K.; Strong, K.; Boersma, F.; et al. Assessment of the quality of tropomi high-spatial-resolution no2 data products in the greater toronto area. *Atmos. Meas. Tech.* **2020**, *13*, 2131–2159, doi:10.5194/amt-13-2131-2020.
30. Eskes, H.J.; van Geffen, J.; Boersma, K.F.; Eichmann, K.U.; Apituley, A.; Pedergnana, M.; Sneep, M.; Veefkind, J.P.; Loyola, D. *S5P/TROPOMI Level-2 Product User Manual Nitrogen Dioxide*; S5P-KNMI-L2-0021-MA, ESA, available at: http://www.tropomi.eu/documents/pum/, last access: 2 June 2020, 2020;
31. Segers, A. Data assimilation in atmospheric chemistry models using Kalman filtering, Ph.D. thesis, Delft University, Netherlands, 2002.
32. Jazwinski, A.H. *Stochastic processes and filtering theory*; Number 64 in Mathematics in science and engineering, Acad. Press, New York, NY (1970);
33. Shin, S.; Kang, J.S.; Jo, Y. The Local Ensemble Transform Kalman Filter (LETKF) with a Global NWP Model on the Cubed Sphere. *Pure Appl. Geophys.* **2016**, *173*, 2555–2570, doi:10.1007/s00024-016-1269-0.
34. Curier, R.L.; Timmermans, R.; Calabretta-Jongen, S.; Eskes, H.; Segers, A.; Swart, D.; Schaap, M. Improving ozone forecasts over Europe by synergistic use of the LOTOS-EUROS chemical transport model and in-situ measurements. *Atmos. Environ.* **2012**, *60*, 217–226, doi:10.1016/j.atmosenv.2012.06.017.
35. Syrakos, A.; Efthimiou, G.C.; Lappas, A.; Sfetsos, A.; Gounaris, N.; Politis, M.; Bartzis, J.G.; Sotiropoulos, D.; Kotzinos, K.; Nikolaou, G.; et al. Assessment of the performance of the UoWM MM5-smoke-CMAQ operational system for west Macedonia. In Proceedings of the HARMO 2010 - Proceedings of the 13th International Conference on Harmonisation within Atmospheric Dispersion Modelling for Regulatory Purposes; 2010; pp. 200–204.
36. Ott, E.; Hunt, B.R.; Szunyogh, I.; Zimin, A. V.; Kostelich, E.J.; Corazza, M.; Kalnay, E.; Patil, D.J.; Yorke, J.A. A local ensemble Kalman filter for atmospheric data assimilation. *Tellus, Ser. A Dyn. Meteorol. Oceanogr.* **2004**, *56*, 415–428, doi:10.1111/j.1600-0870.2004.00076.x.